Journal of Sound and Vibration 329 (2010) 4617–4633

Contents lists available at ScienceDirect

Journal of Sound and Vibration

journal homepage: www.elsevier.com/locate/jsvi

Analytical modeling of squeeze film damping for rectangular elastic plates using Green's functions

M.M. Altuğ Bıçak *, M.D. Rao

Department of Mechanical Engineering - Engineering Mechanics, Michigan Technological University, 1400 Townsend Drive Houghton, MI 49931-1295, USA

ARTICLE INFO

Article history:
Received 14 August 2009
Received in revised form
11 May 2010
Accepted 12 May 2010
Handling Editor: L. Huang
Available online 31 May 2010

ABSTRACT

An analytical method for the solution of squeeze film damping based on Green's function to the nonlinear Reynolds equation considering an elastic plate is presented. This allows calculating the stiffness and damping forces rapidly for various boundary conditions. The elastic plate velocity is applied to the nonlinear Reynolds equation as a forcing term. The nonlinear Reynolds equation is divided into multiple linear nonhomogeneous Helmholtz equations, which then can be solvable using the presented approach. Approximate mode shapes of a rectangular elastic plate are used, enabling the calculation of the damping ratio and frequency shift for the linear case, as well as the complex resistant pressure, for both linear and nonlinear cases.

1. Introduction

Squeeze film damping (SFD) occurs when a plate moves in close proximity to another surface, in effect alternately stretching and squeezing any fluid that may be present in the space between the moving plates. The fluid can act as a mass, spring and damper, having a significant effect on the dynamics of the moving plates. The primary goal of a fluid film damping system is to limit the vibration of a given structure by dissipating the energy to the fluid within the film. However, in micro-electromechanical systems (MEMS) and micro-opto-electromechanical systems, the SFD impacts the operating behavior such as in microswitches, microsensors, microaccelerometers, telescope mirrors [1], etc. From a vibrational point of view, the SFD is a very useful and cost-effective solution to most vibration and vibration-caused noise reduction problems.

Extensive literature has already been developed for the SFD effect relating to air film lubrication [2], which has application in air bearing and levitation systems. The squeeze film analysis of the fluid is covered by three classes of models, the standard Helmholtz equation model, the low reduced frequency model and the Navier–Stokes model.

Darling et al. [3] used the linearized Reynolds equation to calculate the additional spring and damping force acting on the plate using Green's function. Ingard et al. [4] used the wave equation approach under the small amplitude assumption. Using the wave equation and statistical energy analysis, Chow et al. [5] predicted the damping well above the critical frequency of the thick plate. However, the loss factor calculations for the statistical energy analysis are based on the impedance approach which needs the pressure distribution to be calculated in advance.

Maidanik et al. [6] used the simplified Navier–Stokes equation approach with the incompressible fluid assumption. However, the validity of this assumption is restricted to very low frequencies. Önsay [7] and Fox et al. [8] developed fully coupled models including viscothermal effects. Beltman [9] considered viscothermal effects by the full linearized

* Corresponding author.
E-mail address: mmbicak@mtu.edu (M.M. Altuğ Bıçak).

0022-460X/$ - see front matter © 2010 Elsevier Ltd. All rights reserved.
doi:10.1016/j.jsv.2010.05.008

Navier–Stokes problem and low reduced frequency model, and investigated a spherical resonator [10]. Basten et al. [11] applied the low reduced frequency solution of Beltman et al. [9] to calculate the acousto-elastic behavior of double-wall panels. Readers should refer to Refs. [9,11] for an extensive literature review. Moreover, Beltman [9] developed a viscothermal acoustic finite element which models the effects of inertia, viscosity, compressibility and thermal conductivity. Akrout et al. [12] applied this development to two laminated glass plates enclosing a thin viscothermal fluid cavity. Lei et al. [13] developed a three-dimensional viscous finite element model for the analysis of the acoustic fluid–structure interaction systems including the cochlear-based transducers which consists of a three-dimensional viscous acoustic fluid medium interacting with a two-dimensional flat structure domain. Akrout et al. [14] used a modal approach to determine the vibro-acoustic system's response which shows the importance of the viscothermal effects in the case of thin fluid layers.

The Reynolds equation, known from lubrication technology and the theory of rarefied gas physics, is the theoretical background to analyze the SFD effect in this paper. The models that account for flexibility are almost exclusively based on the linearized Reynolds equation or its simplest version—the linearized incompressible Reynolds equation [15]. The models that use the nonlinear Reynolds equation however usually approximate a structure as a one-dimensional beam [16]. The nonlinear Reynolds equation is used in conjunction with the plate equation only in Nayfeh's work [17]. Langlois [2] found damping and spring forces based on squeeze number using a strip plate. Starr [18] noticed the nonlinear effects based on amplitude [19] and gave an approximate formula in order to calculate the nonlinear damping force based on the constant deformation of an oscillating plate. The effects of the boundary condition and the mode shape of the oscillating plate are usually ignored while calculating the viscous forces in MEMS area. The common approach is to minimize the damping force in order to reduce the effect of damping on the operating behavior. Because of this, many researchers analyzed a plate with multiple holes with varying geometry [20–22].

The SFD of parallel plate and basic damping effect can be explained using the modal theory. The resistive force to the plate oscillating normally against the stationary plate is caused by the pressure distribution between plates. Generally, if the plate oscillates with a low frequency, the fluid is not compressed considerably. In this case, there might be an additional mass loading due to the air pumping mechanism. However, if the oscillation frequency of the plate is high, the air fails to escape resulting of the elastic force domination. The Reynolds equation is not valid for high frequencies since the Reynolds equation does not include inertial terms. The measure of applicability of the Reynolds equation can be found by comparing inertial forces with viscous forces. Gross [23] defined the validity of the Reynolds equation by using the modified Reynolds number (Re^*) which is defined by the ratio of the inertial force to the viscous force. According to this approach, the Reynolds equation is valid for $Re^* \ll 1$ since the Poiseuille velocity profile along the gap is assumed. The usage of the low reduced frequency model derived from viscothermal models [9,24], covers both the Reynolds equation and the wave equation using shear wavenumbers.

This paper reports results of a theoretical analysis for the SFD effect on a flexible plate using Green's function. The attached plate mode shapes are applied to the nonlinear Reynolds equation as a forcing term for the fluid to calculate the nonlinear spring and damping forces. For the purpose of this investigation, this can be accomplished by affixing a cover plate over the vibrating structure while leaving a thin air gap between the two pieces. Attaching a new elastic system to the vibrating structure can be thought as the tuned mass damper. However, unlike in the tuned mass damper, the SFD is effective over large bandwidth instead of one particular frequency.

The harmonic solution of the nonlinear Reynolds equation is presented in this work. The general solution of the nonlinear Reynolds equation is divided into each harmonic subproblem. It is also shown that each harmonic problem is dependent upon the solutions of previous harmonics. Using the general solution of the Helmholtz equation, the solution to each harmonic problem can be found using Green's functions. Particular solutions of the nonhomogeneous Helmholtz equation require the input mode shape which can be calculated using biharmonic plate expressions. Using the approximate mode shapes of a rectangular elastic plate, the damping ratio and frequency shift for the linear case, as well as the complex resistant pressure, for both linear and nonlinear cases are calculated.

2. The nonlinear Reynolds equation solution

The fluid flow in continuum regime is governed by the continuity equation and the Navier Stokes momentum equations which are valid for unsteady, compressible and viscous flow. For a small air-gap separating the two plates, the squeeze film flow is predominantly two dimensional (e.g. in the x–y plane). Under following assumptions

- No external forces act on the film.
- No inertial effects exist.
- The structure oscillates with small amplitude and the main flow is driven by pressure gradients in the x and y directions.
- No slip flow occurs at the planar boundaries.
- No variation of pressure across the fluid film.
- The flow is laminar; no vortex flow and no turbulence occur anywhere in the film.
- Fully developed flow is considered within the gap.

- Different assumptions can also be considerable for specific type of fluid. For air, flow is assumed to be isothermal, i.e. ($p \propto \rho$).

The nonlinear Reynolds equation is

$$\nabla \cdot \left(\frac{ph^3}{12\mu} \nabla p \right) = \frac{\partial}{\partial t}(ph) \tag{1}$$

where ∇p is the gradient of the pressure, h is the thickness of the film, and μ is the fluid viscosity. At low ambient pressure or in very thin films, when the mean free path length of the gas is not negligible compared with the film gap h, molecular interactions with the surfaces need to be taken into account. The theory of rarefied gas flow was developed by Knudsen in the early 1900s. Veijola [25] has given a function that approximates the pressure and film width dependency of the viscosity in narrow gaps by

$$\mu_{eff} = \frac{\mu}{1 + 9.658 Kn^{1.159}} \tag{2}$$

where Kn is the Knudsen number defined as $Kn = \lambda/h$, where λ is the mean free path of molecules and h is the gap distance. Based on different derivation considerations, one can get a different viscosity definition such as in [26]. The mean free path of air molecules at ambient pressure P_a is about 65 nm.

The Reynolds equation is applicable only in the continuum flow regime; the relationship between the Knudsen number and flow regimes is shown at Table 1. The effective dynamic viscosities are also tabulated to show the effect of the flow regime on the viscosity.

Under the assumption of harmonically varying gap thickness with the frequency of ω (rad/s), the following equation is defined:

$$h(x,y,t) = h_0(1 + \delta \Phi(x,y) e^{j\omega t}) \tag{3}$$

where Φ is the function of x,y which is the deflection shape of the structure, δ is the dimensionless vibration amplitude which is smaller than 1 and ω is the angular frequency. Since Eq. (1) is nonlinear, harmonics of ω will appear in the pressure solution. So the pressure can be assumed as

$$p(x,y,t) = P_a \left(1 + \sum_{r=1}^{\infty} a_r(x,y) e^{jn\omega t} \right) \tag{4}$$

where $a_r(x,y)$ is the coefficient for the rth harmonic, which is also complex.

If Eqs. (3) and (4) are put into Eq. (1), it can be rewritten as

$$\frac{\partial}{\partial x} \sum_{k=1}^{\infty} \sum_{r=k}^{\infty} \Upsilon \frac{\partial a_{r-k+1}}{\partial x} e^{jr\omega t} + \frac{\partial}{\partial y} \sum_{k=1}^{\infty} \sum_{r=k}^{\infty} \Upsilon \frac{\partial a_{r-k+1}}{\partial y} e^{jr\omega t} = \frac{1}{\sigma} \sum_{r=1}^{\infty} rj\omega (a_r + a_{r-1}\delta\Phi) e^{jr\omega t} \tag{5}$$

where σ is the squeeze number per unit area,

$$\sigma = \frac{12\mu_{\text{eff}}\omega}{h_0^2 P_a} \tag{6}$$

and

$$\Upsilon = a_{r-1} + 3\delta\Phi a_{r-2} + 3\delta^2\Phi^2 a_{r-3} + \delta^3\Phi^3 a_{r-4} \tag{7}$$

The complex coefficients for the zero and negative values of r are therefore,

$$a_0 = 1, \quad a_r = 0 \ \text{ for } r < 0 \tag{8}$$

In order to get the squeeze number which is reported in the literature [16,25], Eq. (6) should be multiplied by the total area of the plate, i.e $L_x L_y$. The first three harmonics of the Eq. (5) can be written as Eqs. (9)–(11) respectively as

$$\frac{\partial^2 a_1}{\partial x^2} + \frac{\partial^2 a_1}{\partial y^2} = j\sigma(a_1 + \delta\Phi) \tag{9}$$

Table 1
The Knudsen number and the corresponding flow regimes.

Knudsen number (Kn)	Flow regime	μ_{eff}/μ
$Kn < 0.01$	Continuum	$0.956 < \mu_{\text{eff}}/\mu < 1$
$0.01 < Kn < 0.1$	Slip	$0.6 < \mu_{\text{eff}}/\mu < 0.956$
$0.1 < Kn < 10$	Transitional	$0.007 < \mu_{\text{eff}}/\mu < 0.6$
$Kn > 10$	Molecular	$0 < \mu_{\text{eff}}/\mu < 0.007$

$$\frac{\partial}{\partial x}\left[\frac{\partial a_2}{\partial x}+(a_1+3\delta\Phi)\frac{\partial a_1}{\partial x}\right]+\frac{\partial}{\partial y}\left[\frac{\partial a_2}{\partial y}+(a_1+3\delta\Phi)\frac{\partial a_1}{\partial y}\right]=2\mathrm{j}\sigma(a_2+a_1\delta\Phi) \tag{10}$$

$$\frac{\partial}{\partial x}\left[\frac{\partial a_3}{\partial x}+(3\delta\Phi+a_1)\frac{\partial a_2}{\partial x}+(3\delta^2\Phi^2+a_1 3\delta\Phi+a_2)\frac{\partial a_1}{\partial x}\right]+\frac{\partial}{\partial y}\left[\frac{\partial a_3}{\partial y}+(3\delta\Phi+a_1)\frac{\partial a_2}{\partial y}+(3\delta^2\Phi^2+a_1 3\delta\Phi+a_2)\frac{\partial a_1}{\partial y}\right]=3\mathrm{j}\sigma(a_3+a_2\delta\Phi) \tag{11}$$

These nonhomogeneous Helmholtz equations (9)–(11) can be solved using Green's functions exactly for the uniform deflection profiles. However, only the first harmonic solution is published in the literature [3]. In the present study, more complicated and realistic plate deflections are considered and the modal force approach is presented. Once the first harmonic equation is solved using Green's functions, Fourier series or numerical methods, the second harmonics can be solved using the first harmonic solution. Moreover, higher harmonics can also be sequentially solved since all the equations are the nonhomogeneous Helmholtz equations, of which the forcing term is already calculated.

2.1. Solution using Green's function

Darling et al. [3] showed the use of Green's function to solve the linearized nonhomogeneous Reynolds equation. Compact analytical models were also presented considering the rigid uniform and the tilting motion of the plate. However, the mode shapes of the rectangular plates are not considered. This present study is the extension of the solution to the elastic models of plates considering the nonlinear Reynolds equation.

The general solution to the linearized Reynolds equation can be given using an infinite series as

$$a_1(x,y)=\sum_m^\infty\sum_n^\infty b_{mn}f_m(x)g_n(y) \tag{12}$$

where $f_m(x)$ and $g_n(y)$ are the harmonic functions of x and y respectively which satisfy the boundary conditions, and b_{mn} is a complex constant coefficient. The derivative of $f_m(x)$ and $g_n(y)$ are

$$\frac{\partial^2 f_m(x)}{\partial x^2}=-m^2\alpha^2 f_m(x) \quad \text{and} \quad \frac{\partial^2 g_n(y)}{\partial y^2}=-n^2\beta^2 g_n(y) \tag{13}$$

where m and n are the integer numbers that can be odd or even based on the boundary configuration, α and β are the multipliers of x and y inside the functions f_m and g_n. If the deflection shape Φ of the plate is expanded to the same series such as

$$\Phi(x,y)=\sum_m^\infty\sum_n^\infty \varepsilon_{mn}f_m(x)g_n(y) \tag{14}$$

the following relationship can be obtained by putting Eqs. (12) and (14) into (9),

$$b_{mn}=\frac{-\mathrm{j}\sigma\delta}{m^2\alpha^2+n^2\beta^2+\mathrm{j}\sigma}\varepsilon_{mn} \tag{15}$$

If the same procedure is applied for the second harmonic, considering the expansion on the same $f_m(x)$ and $g_n(y)$ functions,

$$R(x,y)=\sum_m^\infty\sum_n^\infty r_{mn}f_m(x)g_n(y) \tag{16}$$

$$r_{nm}=\int_0^{L_y}\int_0^{L_x} Rf_m(x)g_n(y)\,\mathrm{d}x\,\mathrm{d}y \tag{17}$$

where the known forcing function R is

$$R=b_{mn}\{(b_{mn}+3\delta\varepsilon_{mn})(f_m'^2g_n^2+f_m^2g_n'^2-\vartheta f_m^2g_n^2)-2\mathrm{j}\sigma\delta\varepsilon_{mn}f_m^2g_n^2\} \tag{18}$$

where f_m' and g_n' are the derivative, w.r.t. its independent variable, and $\vartheta=m^2\alpha^2+n^2\beta^2$. In this case, the complex constant coefficient of the second harmonic turns into

$$c_{mn}=\frac{r_{nm}}{m^2\alpha^2+n^2\beta^2+2\mathrm{j}\sigma} \tag{19}$$

where $a_2(x,y)=\sum_m^\infty\sum_n^\infty c_{mn}f_m(x)g_n(y)$.

The generalized pressure solution to the rth harmonic can also be given in a similar form as in Eq. (12):

$$a_r(x,y)=\sum_m^\infty\sum_n^\infty d_{mk}^r f_m(x)g_k(y) \tag{20}$$

where d_{mn}^r represents the rth harmonic complex constant coefficient which can be obtained as

$$d_{mn}^r = \frac{s_{mn}}{m^2\alpha^2 + n^2\beta^2 + rj\sigma} \tag{21}$$

in which s_{mn} represents the coefficients of the residual known term expansion which is dependent upon the solutions of all harmonics up to the rth harmonic.

The pressure domain solution for the first harmonic equation (12) can be represented in compact form using Green's function also as

$$a_1(x,y) = \int_0^{L_y}\int_0^{L_x} \Phi(\xi,\eta)G(x,y,\xi,\eta)\,d\xi\,d\eta \tag{22}$$

where G is Green's function

$$G(x,y,\xi,\eta) = \sum_m^\infty \sum_n^\infty \varepsilon_{mn} f_m(x)g_n(y)f_m(\xi)g_n(\eta) \tag{23}$$

where ε_{mn} is a multiplier which is dependent upon m,n,ω and σ.

If the deflection of the plate Φ is one of the mode shapes of the plate $\Phi = \Phi_m$, the modal force can be written using the pressure solution as

$$N = \int_0^{L_y}\int_0^{L_x} \Phi_m(x,y)p(x,y)\,dx\,dy \tag{24}$$

If the mode shape Φ_m is selected as orthonormal, which satisfies

$$\int_0^{L_y}\int_0^{L_x} \rho\Phi_m(x,y)\Phi_m(x,y)\,dx\,dy = 1 \tag{25}$$

where ρ is the mass per unit area of the plate. The modal force for the first harmonic solution (N_1) of the pressure can be obtained as

$$N_1 = \sum_m^\infty \sum_n^\infty \frac{-j\sigma\delta}{m^2\alpha^2 + n^2\beta^2 + j\sigma}\varepsilon_{mn}^2 \tag{26}$$

The modal forces for the rth harmonic can now be written as in a generalized form as

$$N_r = \sum_m^\infty \sum_n^\infty \frac{s_{mn}}{m^2\alpha^2 + n^2\beta^2 + rj\sigma}\varepsilon_{mn} \tag{27}$$

2.2. Range of applicability

In 1962, Langlois [2] derived the general form of the Reynolds equation based on the Navier–Stokes equations and the general equations of hydrodynamics. The Reynolds equation is obtained under the condition that the modified Reynolds number is much smaller than unity. The Reynolds equation is not valid for high frequencies since it does not include inertial terms. The measure of applicability of the Reynolds equation can be found by comparing inertial forces with viscous forces per volume [23],

$$Re^* = \frac{\text{inertial force}}{\text{viscous force}} = \frac{\rho u(\partial u/\partial n)}{\mu(\partial^2 u/\partial z^2)} \tag{28}$$

where u is the fluid flow velocity in the direction of n. Assuming the Poiseuille velocity profile along the gap and the direction n as the x-axis, the following formula can be obtained for the fluid flow velocity:

$$u = \frac{hz(\partial p/\partial x)}{2\mu}\left(1 - \frac{z}{h}\right) \tag{29}$$

where z is the direction along the gap. The modified Reynolds number is defined as

$$Re^* = \frac{\rho\omega h_0^2}{\mu} \ll 1 \tag{30}$$

which should be smaller than unity for any point underneath the plate. The modified Reynolds number can be rewritten using the squeeze number as

$$Re^* = \frac{\rho P_a h_0^4}{12\mu^2}\sigma \tag{31}$$

The modified Reynolds number formula considering the journal bearings can be found in Ref. [23].

3. Calculation of squeeze film stiffness and damping

According to the analysis of Langlois [2], and Griffin et al. [27], squeeze film air provides extra damping and stiffness force to the system. For a finite element modeled system, one can get mass, stiffness and damping matrices as

$$M\ddot{x}+Kx=f(x,\dot{x}) \tag{32}$$

Eq. (32) can be expressed in terms of modal vectors, $x(t)=\Phi_m\varphi(t)$ in which Φ_m represents modal vector as follows:

$$\ddot{\varphi}+\omega_n^2\varphi=\Phi_m^{\mathrm{T}}f(\Phi_m\varphi,\Phi_m\dot{\varphi}) \tag{33}$$

where ω_n and $\varphi(t)$ represent the natural frequency and modal coordinates. For a continuous system, Eq. (33) can be written as

$$\ddot{\varphi}+\omega_n^2\varphi=\int_\Omega \Phi_m f(\Phi_m\varphi,\Phi_m\dot{\varphi})\,\mathrm{d}\Omega \tag{34}$$

where Ω represents the solution domain. After the calculation of the modal forcing term, the imaginary part can be converted into the velocity component using the relationship $\dot{\varphi}=\mathrm{j}\omega\varphi$.

The right hand side of Eq. (34), the modal force provides two components the in-phase and the out-of-phase which can be decomposed as $\Phi_m^{\mathrm{T}}f=-F_k\varphi-F_d\dot{\varphi}$. Considering a single degree of freedom system, the damping ratio and the natural frequency shift can be found as

$$\zeta=\frac{1}{2\omega_n}F_d \tag{35}$$

$$\Delta\omega=\sqrt{\omega_n^2+F_k}-\omega_n \tag{36}$$

The damping ratio and the frequency shift formulations are based on the linear pressure solution, hence it cannot be applicable to nonlinear cases. The mass normalized mode shapes are used in order to calculate the modal damping and the frequency shift using Eqs. (35) and (36). The other way to calculate the damping ratio and the frequency shift is to use the time integration technique and then calculating the phase difference. However, the nonlinearity or higher harmonics cannot be captured since the stiffness and the damping are calculated based on the phase difference between the velocity and the pressure. Moreover, the sucking and squeezing motions create unequal fluctuations around the ambient pressure.

4. Examples

To illustrate the details of the pressure and modal force solution, the transverse motion of a plate is considered. The problem domain is selected as $0\leqq x\leqq L_x$ and $0\leqq y\leqq L_y$ corresponding to a rectangular plate of dimensions L_x,L_y. The proper Green's function is constructed and used for each different case. For the structural modal solution, approximate mode shapes for Poisson's ratio is 0.25 which can be found in Ref. [28] are used. Tabulated mode shapes are calculated approximately using the Rayleigh method. In order to solve the problem defined by Eq. (5), boundary conditions should be defined. For the boundary edges there are two different boundary conditions:

- Boundary point is open to ambient pressure $p=P_a$.
- Pressure gradient is zero, or closed end $\partial p/\partial n=0$ where n is the outwards normal vector at the boundary.

The structural boundary conditions for the plate edges are represented by four letters. For example, CFCS stands for clamped–free–clamped–simply supported plate for bottom ($y=0$), right ($x=L_x$), upper ($y=L_y$) and left edges ($x=0$). It is assumed that the pressure gradient is zero for simply supported and clamped edges, whereas the boundary condition is open to ambient air for the free edge. All investigated mode shapes are shown at Table 2.

The first harmonic solution to the nonlinear Reynolds equation is presented in the following subsections. The second harmonic solutions can be found in the Appendices.

4.1. Exact solution for clamped boundary conditions (CCCC)

For the clamped boundaries case, the approximate normalized mode shape [28] using the Rayleigh method is given as

$$\Phi(x,y)=\left(\cos\frac{2\pi x}{L_x}-1\right)\left(\cos\frac{2\pi y}{L_y}-1\right) \tag{37}$$

The first-order pressure a_1 can be written using Eq. (12) where

$$f(x)=\cos\frac{2\pi mx}{L_x},\quad g(y)=\cos\frac{2\pi ny}{L_y} \tag{38}$$

Table 2
Mode shapes.

Configuration	Deflection shape $\Phi(x,y)=\Phi_m(x,y)$
CCCC	$\left(\cos\frac{2\pi x}{L_x}-1\right)\left(\cos\frac{2\pi y}{L_y}-1\right)$
CFCC	$\left(1-\cos\frac{\pi x}{2L_x}\right)\left(\cos\frac{2\pi y}{L_y}-1\right)$
FCFC	$\left(1-\cos\frac{2\pi x}{L_x}\right)$
FSFS	$\left(\sin\frac{\pi x}{L_x}\right)$
CFFC	$\left(1-\cos\frac{\pi x}{2L_x}\right)\left(1-\cos\frac{\pi y}{2L_y}\right)$
FFFC	$\left(1-\cos\frac{\pi x}{2L_x}\right)$

Since the mode shape can be represented by using only four terms of the entire series, the solution of the nonhomogeneous Helmholtz equation yields only four terms. Using the solution, the nondimensional pressure can be calculated as follows:

$$a_1(x,y)=\delta\left(-1+\frac{\mathrm{j}\sigma}{\alpha^2+\mathrm{j}\sigma}f_1(x)+\frac{\mathrm{j}\sigma}{\beta^2+\mathrm{j}\sigma}g_1(y)-\frac{\mathrm{j}\sigma}{(\alpha^2+\beta^2)+\mathrm{j}\sigma}f_1(x)g_1(y)\right) \tag{39}$$

where $\alpha=2\pi/L_x$, $\beta=2\pi/L_y$, $f_1(x)=\cos\alpha x$ and $g_1(y)=\cos\beta y$. And modal force can be obtained as using the orthonormalized mode shape equation (37) as

$$N=-\frac{1}{3}\sqrt{\frac{L_xL_y}{\rho}}P_a\delta\left(2+\frac{\mathrm{j}\sigma}{\alpha^2+\mathrm{j}\sigma}+\frac{\mathrm{j}\sigma}{\beta^2+\mathrm{j}\sigma}+\frac{1}{2}\frac{\mathrm{j}\sigma}{\alpha^2+\beta^2+\mathrm{j}\sigma}\right) \tag{40}$$

where ρ is the constant mass density per unit area of the plate.

Unlike the solution which is given by Darling et al. [3], which exhibits the infinite series solution for the uniform plate displacement, the solution to a particular mode shape includes the first couple of terms of the entire series due to the expansion of the mode shape. Darling concluded that the damping mechanism does not exist considering the uniform motion. However, even if all the edges are closed, the pumping mechanism due to the mode shape deflection, exists which creates damping, which is plausible and can be understood by considering the imaginary part of Eqs. (39) and (40).

One can get a similar formula using the low reduced frequency model approach as follows:

$$av_1(x,y)=\frac{\delta}{2}n(s\tilde{\sigma})\left(-1+\frac{\Gamma^2\omega}{\Gamma^2\omega+c_0\alpha^2}f_1(x)+\frac{\Gamma^2\omega}{c_0\beta^2+\Gamma^2\omega}g_1(y)+\frac{\Gamma^2\omega}{c_0(\beta^2+\alpha^2)+\Gamma^2\omega}f_1(x)g_1(y)\right) \tag{41}$$

where av_1 is the pressure solution of the first harmonic to the low reduced frequency model, $s=\frac{1}{2}h_0\sqrt{\rho\omega/\mu}$ is the shear wavenumber, Γ is the propagation constant, c_0 is the velocity of the sound, $n(s\tilde{\sigma})=(1+((\gamma-1)/\gamma)B(s\tilde{\sigma}))^{-1}$, $B(s\tilde{\sigma})=\tanh(s\sqrt{\mathrm{j}})/s\sqrt{\mathrm{j}}-1$, γ is the ratio of the specific heats, and $\tilde{\sigma}$ is the square root of the Prandtl number. More information about the low reduced frequency model can be found in Ref. [24].

The nonlinear (second harmonic) solution for the CCCC case can be found in Appendix A.

4.2. Case: CFCC

Considering the same plate geometry as before, but a free edge at $y=L_x$, the nondimensional pressure a_1 can be obtained as

$$a_1(x,y)=\sum_m^{\infty}\frac{\mathrm{j}\sigma\delta(-1)^{(m-1)/2}\varepsilon_{mn}}{m\pi}\left(\frac{1}{A_1}-\frac{1}{A_2}\cos\frac{2\pi y}{L_y}\right)\cos\frac{m\pi x}{2L_x} \tag{42}$$

where

$$\varepsilon_{mn}=\begin{cases}-\frac{\pi-4}{2} & m=1\\ 4 & m>1\end{cases}\quad\text{and}\quad A_1=\frac{m^2\pi^2}{4L_x^2}+\mathrm{j}\sigma,\quad A_2=\frac{m^2\pi^2}{4L_x^2}+4\frac{\pi^2}{L_y^2}+\mathrm{j}\sigma,\ \mathrm{j}=\sqrt{-1}\ \text{for}\ m=1,3,5,\ldots.$$

After using the orthonormalized mode shape with a multiplier $\frac{1}{2}\sqrt{3L_xL_y(3\pi-8)/\rho\pi}$, the modal force can be written as

$$N=\sum_m^{\infty}\frac{-\mathrm{j}\sqrt{L_xL_y}P_a\sigma\delta\varepsilon_{mn}}{2\sqrt{3}\pi^2Sm^2\sqrt{\rho}}\left(\frac{1}{A_1}+\frac{1}{2A_2}\right) \tag{43}$$

where

$$\varepsilon_{mn}=\begin{cases}\pi^2-8\pi+16 & m=1\\ 32 & m>1\end{cases}\quad\text{and}\quad S=\sqrt{\frac{3\pi-8}{\pi}}.$$

The nonlinear (second harmonic) solution for this case can be found in Appendix B.

4.3. Case: FCFC and FSFS

Considering the same plate geometry as before, but with the clamped edges, which is the zero flow condition, expressed as $x=0$ and $x=L_x$, and the free edges at $y=0$ and $y=L_x$, the nondimensional pressure can be found as

$$a_1(x,y)=\sum_n^{\infty}\frac{4\mathrm{j}\sigma\delta}{\pi n}\left(\frac{1}{A_1}-\frac{1}{A_2}\cos\frac{2\pi x}{L_x}\right)\sin\frac{n\pi y}{L_y} \tag{44}$$

where $A_1=n^2\pi^2/L_y^2+\mathrm{j}\sigma$ and $A_2=4\pi^2/L_x^2+n^2\pi^2/L_y^2+\mathrm{j}\sigma$ for $n=1,3,5,\ldots$.

Using $\frac{1}{2}(6L_xL_y/\rho)^{1/2}$ as the orthonormal multiplier, one can find the modal force as

$$N=\sum_n^{\infty}\frac{-4\sqrt{2}\mathrm{j}\sqrt{L_xL_y}P_a\sigma\delta}{\sqrt{3}\pi^2n^2\sqrt{\rho}}\left(\frac{2}{A_1}+\frac{1}{A_2}\right) \tag{45}$$

If the simply supported mode shape is used, then the pressure and the modal force turn into

$$a_1(x,y)=\sum_m^{\infty}\sum_n^{\infty}\frac{8\mathrm{j}\sigma\delta\varepsilon_{mn}}{\pi^2(m^2-1)n\left(\frac{m^2\pi^2}{L_x^2}+\frac{n^2\pi^2}{L_y^2}+\mathrm{j}\sigma\right)}\cos\frac{m\pi x}{L_x}\sin\frac{\pi ny}{L_y} \tag{46}$$

$$N=\sum_m^{\infty}\sum_n^{\infty}\frac{-32\sqrt{2}\mathrm{j}\sqrt{L_xL_y}P_a\sigma\delta\varepsilon_{mn}}{\pi^4(m^2-1)n^2\sqrt{\rho}\left(\frac{m^2\pi^2}{L_x^2}+\frac{n^2\pi^2}{L_y^2}+\mathrm{j}\sigma\right)} \tag{47}$$

where

$$\varepsilon_{mn}=\begin{cases}1 & m=1\\ 2 & m>1\end{cases}$$

and the orthonormal multiplier is $\sqrt{L_xL_y/2\rho}$ for $m=0,2,4,\ldots$ and $n=1,3,5,\ldots$.

The nonlinear (second harmonic) solution for this case is presented in Appendices C and D.

4.4. Case: FFFC

In this case, the three edges where $x=L_x$, $y=0$ and $y=L_y$ are considered as open to the ambient air, and the left edge is considered as the zero flow condition at $x=0$, the nondimensional pressure is

$$a_1(x,y)=\sum_m^{\infty}\sum_n^{\infty}\frac{\mathrm{j}\sigma\delta\varepsilon_{mn}}{\pi^2mn\left(\frac{m^2\pi^2}{4L_x^2}+\frac{n^2\pi^2}{L_y^2}+\mathrm{j}\sigma\right)}\cos\frac{m\pi x}{2L_x}\sin\frac{\pi ny}{L_y} \tag{48}$$

where

$$\varepsilon_{mn}=\begin{cases}\dfrac{\pi-4}{4} & m=1\\ (-1)^{(m+1)/2} & m>1\end{cases}\quad\text{for } m=1,3,5,\ldots \text{ and } n=1,3,5,\ldots$$

After using the orthonormalized mode shape with the multiplier $\sqrt{L_xL_y(3\pi-8)/2\rho\pi}$, the modal force can be expressed as

$$N=\sum_m^{\infty}\sum_n^{\infty}\frac{-4\sqrt{2}\mathrm{j}\sqrt{L_xL_y}P_a\sigma\delta\varepsilon_{mn}^2}{\pi^4\sqrt{\frac{3\pi-8}{\pi}}m^2n^2\sqrt{\rho}\left(\frac{m^2\pi^2}{4L_x^2}+\frac{n^2\pi^2}{L_y^2}+\mathrm{j}\sigma\right)} \tag{49}$$

The nonlinear (second harmonic) solution for this case is presented in Appendix F.

4.5. Case: CFFC

Considering the same plate as in FFFC case, but with the clamped edge at $y=0$, the nondimensional pressure a_1 is

$$a_1(x,y)=\sum_m^\infty\sum_n^\infty \frac{-\mathrm{j}\sigma\delta\varepsilon_m\varepsilon_n}{\pi^2 mn\left(\frac{m^2\pi^2}{4L_x^2}+\frac{n^2\pi^2}{4L_y^2}+\mathrm{j}\sigma\right)}\cos\frac{m\pi x}{2L_x}\cos\frac{\pi n y}{2L_y} \tag{50}$$

where

$$\varepsilon_m=\begin{cases}\dfrac{\pi-4}{4} & m=1\\ (-1)^{(m+1)/2} & m>1\end{cases}\quad\text{and}\quad \varepsilon_n=\begin{cases}\dfrac{\pi-4}{4} & n=1\\ (-1)^{(n+1)/2} & n>1\end{cases}\quad\text{for } m=1,3,5,\ldots \text{ and } n=1,3,5,\ldots$$

The modal force can be obtained after using the orthonormalized mode shape with the multiplier $((3\pi-8)/2)\sqrt{L_xL_y/\rho\pi}$ as

$$N=\sum_m^\infty\sum_n^\infty \frac{-32\mathrm{j}\sqrt{L_xL_y}P_a\sigma\delta\varepsilon_m^2\varepsilon_n^2}{\pi^3(3\pi-8)m^2n^2\sqrt{\rho}\left(\frac{m^2\pi^2}{4L_x^2}+\frac{n^2\pi^2}{L_y^2}+\mathrm{j}\sigma\right)} \tag{51}$$

The nonlinear (second harmonic) solution for this case is presented in Appendix E.

5. Comparison of cases

5.1. Linear (First harmonic) comparisons

In this section, the pressure values and modal forces are compared for a square plate $L_x=L_y=1$ m, considering the orthonormalized mode shapes. Readers should divide the mode shapes with its multiplier to replicate the following results. The real and imaginary components of each modal force are plotted in Figs. 1 and 2 as functions of the squeeze number σ defined by Eq. (6) and compared with the solution of Darling et al. [3] in which deflection is taken as uniform. While calculating the complex resistance force using Darling's formula, the total mode deflection is used as the uniform deflection amplitude. The mass density per unit area ρ is selected as $1\,\mathrm{kg/m^2}$ in order to compare with the literature results. Moreover, the frequency shift and the damping ratio are also evaluated and plotted in Fig. 3 for each case using Eqs. (35) and (36) considering ω is changed inside Eq. (6). The other parameters used in the calculations are

$$P_a=100\,\mathrm{kN/m^2},\quad \mu=2\times10^{-5}\,\mathrm{N\,s/m^2},\quad h_0=0.1\,\mathrm{mm} \tag{52}$$

and $\sigma=(\omega/4)\,\mathrm{s/m^2}$. The modified Reynolds number for the examples are $Re^*=\sigma/400$, which validates the results up to $\sigma=400\,\mathrm{m^{-2}}$ (2.6 in the Log scale).

The normalized stiffness force for different boundary conditions are presented with the literature results [3] in Fig. 1. It is interesting to note that the stiffness force converges to 0.45 for the CCCC case and goes to 1 where the theoretical limit

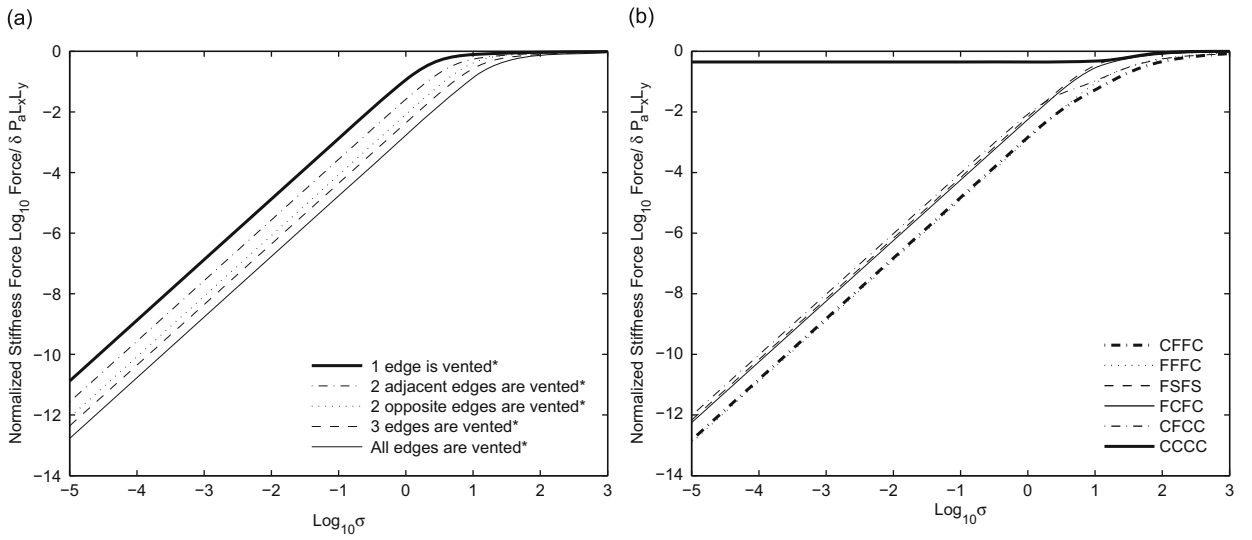

Fig. 1. Normalized spring force for different boundary conditions of a square plate: (a) [3] for constant uniform deflection, (b) present study.

for high σ values. Fig. 1(b) depicts that the normalized stiffness force remains constant for CCCC unlike vented cases, while vibration frequency ω is decreasing. This trend is clearly the same as in Fig. 1(a) and the order of ventilation cases are the same. For the vented cases, the low frequency force exhibits a directly proportional relationship in the Log–Log scale and the following relationship can be extracted

$$\log_{10}\frac{\text{stiffness force}}{\delta P_a L_x L_y} \simeq \log_{10}\sigma^2 \tag{53}$$

The normalized damping force for both the literature results [3] and the present study results are shown in Fig. 2. It is observable that the damping force increases proportionally with σ values up to a maximum level then decreases gradually. The decreasing trend for the realistic cases in Fig. 2(b) is not the same as for the uniform deflection case in Fig. 2(a). However, the increasing trend in Fig. 2(a) is nearly the same as in Fig. 2(b).

The effects of ω and/or σ on the frequency shift and damping ratio can be seen in Fig. 3. A Log axis is selected in order to capture the effects. Notice that the plate mode shape is assumed unchanged during the calculations of the frequency shift and damping ratio. It is interesting to point out that for all cases except the CCCC case, the frequency shift is directly proportional with σ for low values and inversely proportional for high values of σ. Since the stiffness or the real part of the

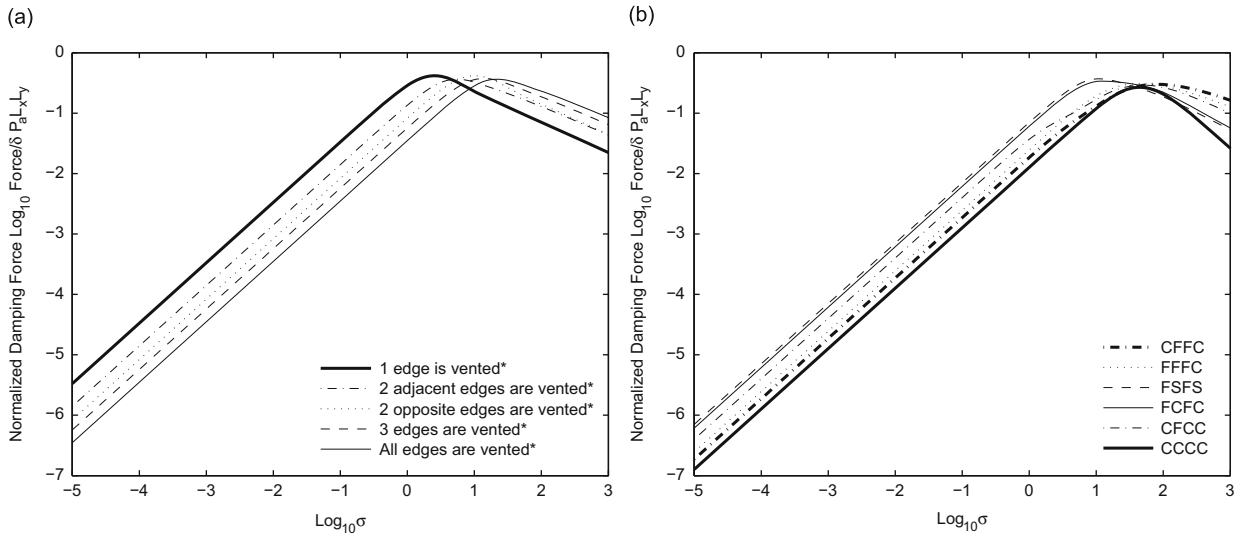

Fig. 2. Normalized damping force for different boundary conditions of a square plate: (a) [3] for constant uniform deflection, (b) present study.

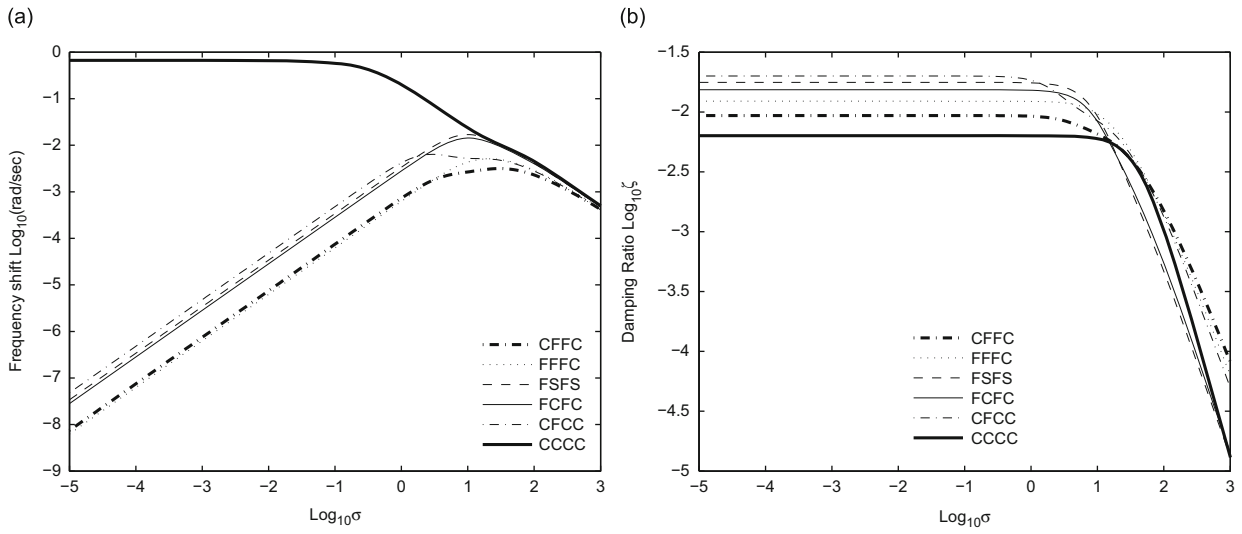

Fig. 3. Frequency shift (a) and damping ratio (b) for various boundary conditions of the square plate.

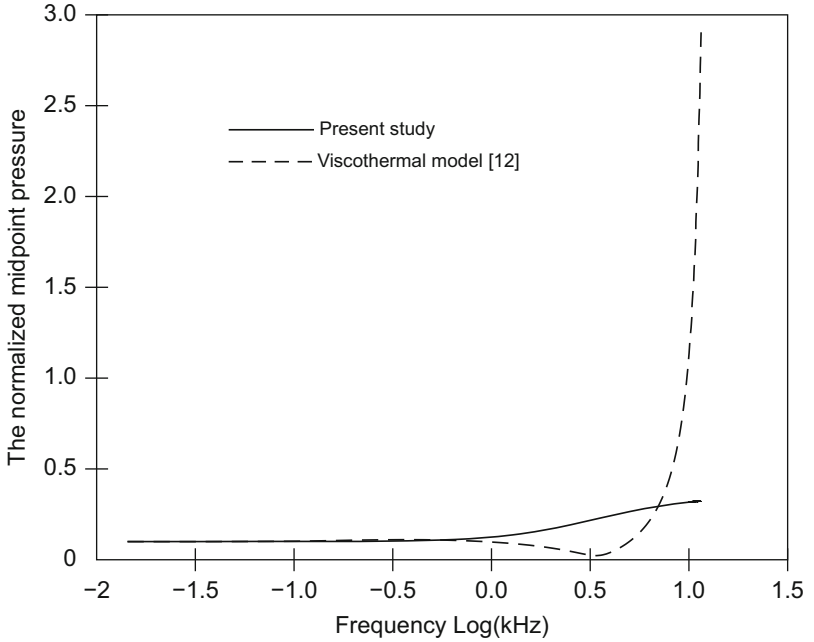

Fig. 4. The midpoint (x,y=0.5 m) absolute pressure variation.

reaction force reaches to steady state of which the impact of frequency shift is reduced. Moreover, unlike vented cases such as CFCC, FCFC, etc. the frequency shift of CCCC is constant up to $\sigma \approx 0.01\,\mathrm{m}^{-2}$. For high values of σ air underneath the plate is getting squeezed, instead of escaping through boundaries which are open to ambient pressure. This phenomenon can also be seen in the damping ratio graph. For very small values of σ, the damping ratio stays constant, which means most of the air can be pumped unlike for high frequencies, at which the pumping effect is reduced and damping is said to be inversely proportional with frequency. These damping evaluations can also be used for the statistical energy analysis purposes under parabolic flow restriction.

The comparison between the viscothermal model [9] and the present study is presented in Fig. 4. The variation of the normalized absolute pressure at the center point of the plate is plotted against frequency.

The pressure calculations become different starting from 100 Hz, the model presented in this study is no longer capable of producing correct results beyond this frequency.

5.2. Nonlinear (second harmonic) comparisons

The capability of the present analysis is further demonstrated by considering the nonlinear analysis of the plate which has the same physical properties as that specified for the previous linear problem. The three cases CCCC, CFCC, and FCFC are investigated. The influence of the nondimensional deflection multiplier δ and σ on the total amount of force of the first and second harmonics are illustrated in Fig. 5. The isopleth map is used to show the total force acting on the plate. As shown in Fig. 5, the effect of the deflection δ on the total force is rather significant. When the σ values are low, the real part of the linear solution Fig. 5(a) is proportionally increasing with increasing δ. The real part of the total force tends to shift for higher values of σ. The real part of the first harmonic total force is nearly directly proportional with the δ in the σ range investigated. However, the real part of the total force due to the second harmonic $\mathrm{Re}(Fa_2)$, presents a different distribution. $\mathrm{Re}(Fa_2)$ is nearly directly proportional with δ for high values of σ, but nearly constant for the lower values. It can be concluded that the nonlinearity of the real part of the total force is rather important for the high values of σ for this case. This phenomenon can also be observed on the imaginary part. Moreover, the optimal damping force of the first and second harmonics in Fig. 5(b,d), can be achieved by adjusting the σ values around $50\,\mathrm{m}^{-2}$.

The plate with CFCC boundary conditions shows different contour lines in Fig. 6. In this case, $\mathrm{Re}(Fa_1)$ and $\mathrm{Re}(Fa_2)$ show similar contour profiles except the magnitudes of the contours. The increase in the second harmonic force $\mathrm{Re}(Fa_2)$ is more than that of the $\mathrm{Re}(Fa_1)$ for high σ values. The imaginary parts $\mathrm{Im}(Fa_1)$ and $\mathrm{Im}(Fa_2)$ exhibit local extremums around $\sigma = 10\,\mathrm{m}^{-2}$ and gradually increase for high values of σ. Unlike in the CCCC case, the stiffness and the damping force increase in the second harmonic due to high values of δ is more than the increase in the first harmonic. It can therefore be concluded that the nonlinearity is more severe than that in the CCCC case.

The results of the plate with FCFC boundary conditions are presented in Fig. 7. The real forces $\mathrm{Re}(Fa_1)$ and $\mathrm{Re}(Fa_2)$, show similar contour profiles but the amplitudes of the contours are different as in the previous case. However, the stiffness force nonlinearity is lower compared to the CFCC case. This can also be observed in the damping forces in Fig. 7(b,d).

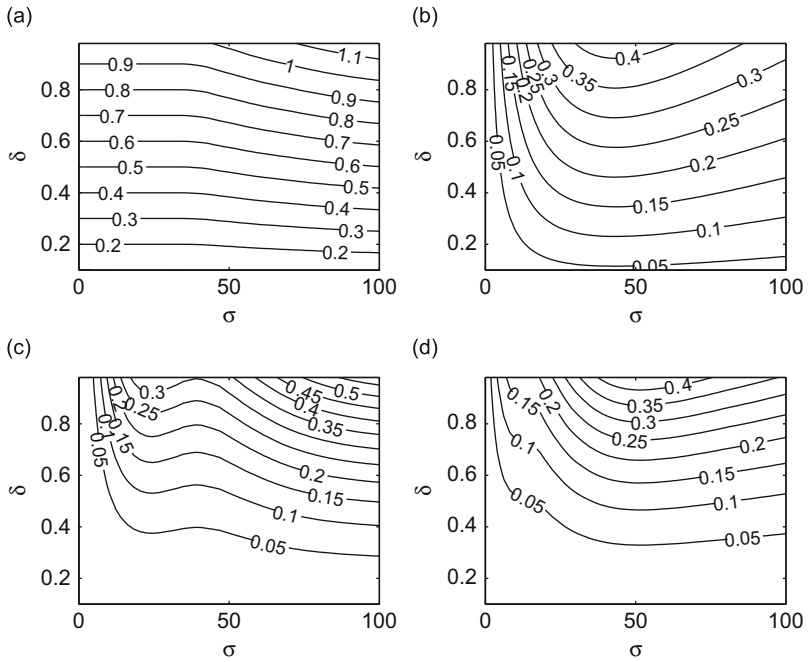

Fig. 5. Total force acting to the plate for CCCC case, real part of a_1=Re(a_1) (a), imaginary part of a_1=Im(a_1) (b), Re(a_2) (c), Im(a_2) (d).

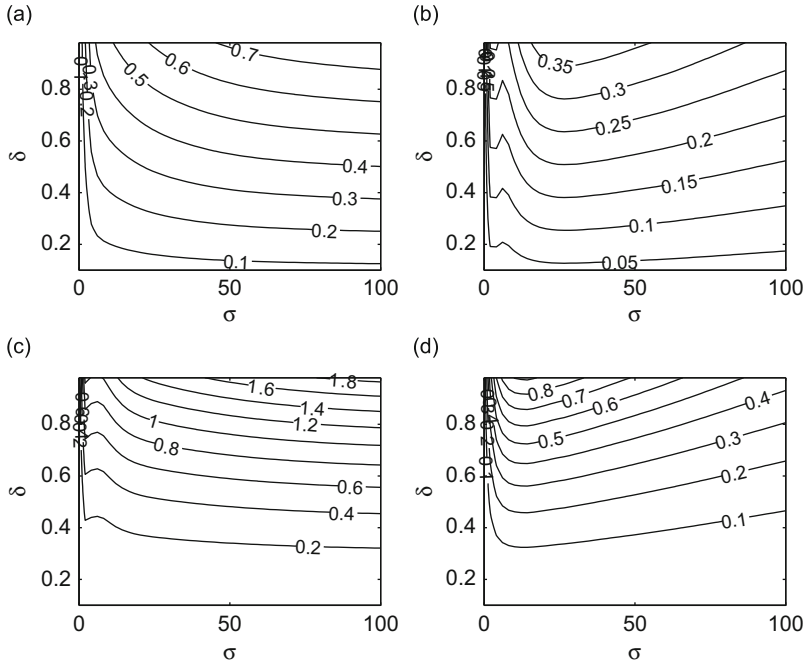

Fig. 6. Total force acting to the plate for CFCC case, Re(a_1) (a), Im(a_1) (b), Re(a_2) (c), Im(a_2) (d).

6. Conclusions

Compact analytical models for computing the effects of compressible SFD are developed using Green's function approach. The coupling is handled by applying the structural velocity distribution to the Reynolds equation as the forcing term. The nonlinear Reynolds equation is divided into the harmonics of the oscillation frequency of the structure. Then the

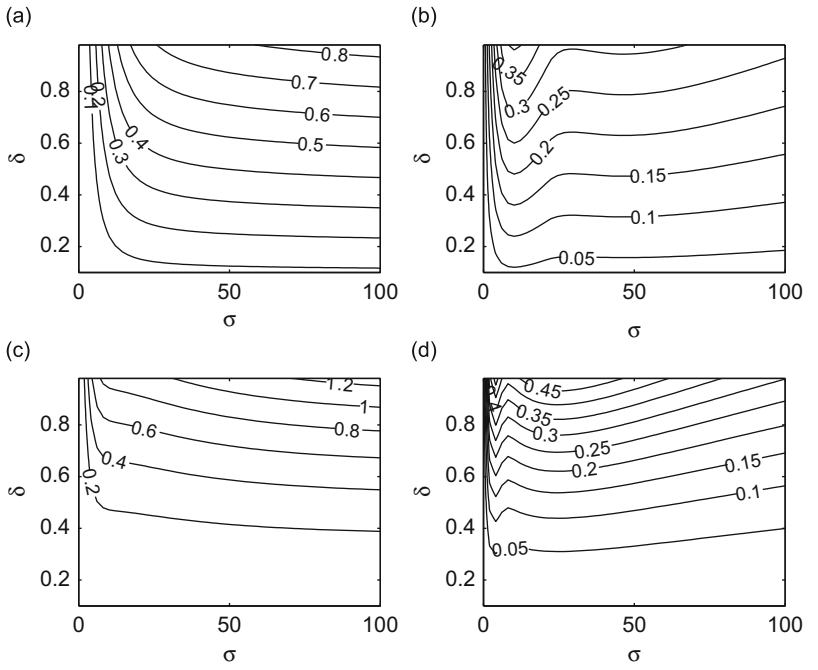

Fig. 7. Total force acting to the plate for FCFC case, Re(a_1) (a), Im(a_1) (b), Re(a_2) (c), Im(a_2) (d).

solution to the Reynolds equation for each harmonic is presented in order to calculate the nonlinear pressure distribution, the nonlinear damping and stiffness forces, as well as the damping ratio and frequency shift for the linear case. The nonlinearity due to the deflection amplitude of the structure and the squeeze number are investigated. It is found that the nonlinearity is directly effected by the boundary conditions for a particular configuration. The presented method allows the rapid calculation of reaction forces using the infinite series which includes the expansion of approximate mode shapes on eigenfunctions. The truncation of infinite series to the first few terms can also be represented, which is useful for system simulations. Tabulated examples can be expandable to cover more complicated and higher mode shapes.

In conclusion, the present analysis provides an efficient and rapid technique for investigating both linear and nonlinear effects of SFD on rectangular elastic plates. Further, it also provides a powerful, compact and convenient tool to identify the modal damping and frequency shift for linear cases as well as pressure distribution underneath plates in practice.

Appendix A. CCCC

Considering

$$a_1(x,y) = \sum_{m=0}^{2}\sum_{n=0}^{2} c_{mn}\cos\frac{m\pi x}{L_x}\cos\frac{n\pi y}{L_y} \tag{54}$$

and

$$a_2(x,y) = \sum_{m=0}^{4}\sum_{n=0}^{4} e_{mn}\cos\frac{m\pi x}{L_x}\cos\frac{n\pi y}{L_y} \tag{55}$$

the second harmonic complex coefficients are

$$e_{00} = -\frac{\delta}{4}(c_{22}-2c_{20}-2c_{02}+4c_{00})$$

$$e_{20} = -\frac{(6\delta c_{20}+c_{02}c_{22}+2c_{00}c_{20}-2\delta c_{22})\pi^2}{\mathrm{i}\sigma L_x^2} + \frac{\delta}{2}(c_{22}-2c_{20}-c_{02}+2c_{00})$$

$$e_{40} = \frac{-(3\delta c_{22}-6\delta c_{20}+2c_{20}^2+c_{22}^2)\pi^2}{iL_x^2\sigma} + \frac{2c_{20}-c_{22}}{4}\delta$$

$$e_{02} = -\frac{(-2c_{00}+c_{20}+2c_{02}-c_{22})\mathrm{i}\delta\sigma L_y^2 + 2(-3\delta c_{22}+c_{22}c_{20}+2c_{00}c_{02}+6\delta c_{02})\pi^2}{4\pi^2+2\mathrm{i}L_y^2\sigma}$$

$$e_{04}=\frac{(2c_{02}-c_{22})\frac{1}{4}\mathrm{i}\sigma\delta L_y^2+(6\delta c_{02}-2c_{02}^2-c_{22}^2-3\delta c_{22})\pi^2}{\mathrm{i}L_y^2\sigma+8\pi^2}$$

$$e_{22}=-\frac{(c_{00}-c_{20}+c_{22}-c_{02})\mathrm{i}\delta L_y^2\sigma+(c_{00}c_{22}+c_{02}c_{20}-3\delta c_{20}+3\delta c_{22})2\pi^2\left(\frac{L_y^2}{L_x^2}+1\right)}{2\pi^2+iL_y^2\sigma}$$

$$e_{42}=-\frac{(c_{20}-c_{22})L_x^2L_y^2\mathrm{i}\delta\sigma+(6\delta c_{20}L_y^2-6\delta c_{22}L_y^2+4c_{20}c_{22}L_y^2+c_{20}c_{22}L_x^2-3\delta c_{22}L_x^2)2\pi^2}{2L_x^2(2\pi^2+\mathrm{i}Ly^2\sigma)}$$

$$e_{24}=-\frac{(c_{02}-c_{22})L_x^2L_y^2\mathrm{i}\delta\sigma+(c_{02}c_{22}Ly^2-3\delta c_{22}L_y^2+4c_{02}c_{22}L_x^2-6\delta c_{22}L_x^2+6\delta c_{02}L_x^2)2\pi^2}{2L_x^2(\mathrm{i}L_y^2\sigma+8\pi^2)}$$

$$e_{44}=-c_{22}\frac{(c_{22}L_y^2+3\delta L_y^2+c_{22}L_x^2+3\delta L_x^2)4\pi^2+\mathrm{i}\sigma\delta L_x^2L_y^2}{4L_x^2(\mathrm{i}L_y^2\sigma+8\pi^2)} \tag{56}$$

Appendix B. CFCC

Considering the first harmonic solution as

$$a_1(x,y)=\sum_m\left(c_m+d_m\cos\frac{2\pi y}{L_y}\right)\cos\frac{m\pi x}{2L_x} \tag{57}$$

and the second harmonic,

$$a_2(x,y)=\sum_m\left(e_m+f_m\cos\frac{2\pi y}{L_y}+g_m\cos\frac{4\pi y}{L_y}\right)\cos\frac{m\pi x}{2L_x} \tag{58}$$

the second harmonic coefficients are

$$e_m=\sum_n\frac{(1+8nm)\frac{\mathrm{i}\sigma\delta}{4\pi}-\frac{3mn\pi\delta}{8L_x^2}(1-n^2-m^2)}{a(n\pm1\pm m)}(d_m-2c_m)+\frac{3\pi\delta mn}{32aL_x^2}(d_m-2c_m)-\sum_n\frac{\pi m^2}{8aL_x^2n}(2c_m^2+d_m^2) \tag{59}$$

where $a=-16\pi L_x^2/m^2\pi^2+8\mathrm{i}L_x^2\sigma$, $(n\pm1\pm m)=(n+1+m)(n+1-m)(n-1+m)(n-1-m)$ and m,n are odd numbers.

$$f_m=b\sum_n\left\{\left(\frac{1}{4}\mathrm{i}\sigma+\frac{3\pi^2}{32L_x^2}m^2\right)(c_m-d_m)-\frac{3\pi^2}{2L_y^2}d_m\right\}\delta(-1)^{(m+1)/2}-\frac{\frac{4}{L_y^2}+\frac{n}{4L_x^2}}{4m^2-n^2}\pi m^2c_md_m$$
$$+\frac{\left(\frac{3\pi}{8L_x^2}(m^2-1+n^2)+\frac{2}{\pi}\mathrm{i}\sigma\right)(c_m-d_m)-\frac{12\pi}{L_y^2}d_m}{(m\pm1\pm n)}mn\delta \tag{60}$$

where $b=-32L_x^2L_y^2/(8\mathrm{i}\sigma L_x^2L_y^2+m^2\pi^2L_y^2+16\pi^2L_x^2)$.

$$h_m=c\sum_n\left(\frac{1}{8}\mathrm{i}\sigma+\frac{3\pi^2}{2L_y^2}+\frac{3\pi^2}{64L_x^2}m^2\right)\delta(-1)^{(m+1)/2}d_m-\frac{\frac{n^2+4m^2}{16L_x^2}+\frac{4}{L_y^2}}{n(4m^2-n^2)}m^2\pi d_m^2+\frac{\frac{\mathrm{i}\sigma}{\pi}+\frac{3\pi}{16L_x^2}(n^2+m^2-1)+\frac{12\pi}{L_y^2}}{(m\pm1\pm n)}mn\delta d_m \tag{61}$$

where $c=-32L_x^2L_y^2/(8\mathrm{i}\sigma L_x^2L_y^2+m^2\pi^2L_y^2+64\pi^2L_x^2)$

Appendix C. FCFC

Considering the first harmonic solution as

$$a_1(x,y)=\sum_m\left(c_m+d_m\cos\frac{2\pi x}{L_x}\right)\sin\frac{m\pi y}{L_y} \tag{62}$$

and the second harmonic,

$$a_2(x,y)=\sum_m\left(e_m+f_m\cos\frac{2\pi x}{L_x}+h_m\cos\frac{4\pi x}{L_x}\right)\sin\frac{m\pi y}{L_y} \tag{63}$$

the coefficients of the second harmonic can be found as

$$e_m=a\left\{\mathrm{i}\sigma+\frac{3\pi^2}{2L_y^2}m^2\right\}\delta(d_m-2c_m)-a\sum_{n,g}\frac{(d_gd_n-2c_gc_n)+c_n(g^2+n^2-m^2)(c_g+\frac{1}{2}d_g)}{(n\pm g\pm m)}\frac{\pi}{L_y^2}gmn \tag{64}$$

where $a=L_y^2/(2i\sigma L_y^2+m^2\pi^2)$ and n,g are odd numbers.

$$f_m=b\left(2i\sigma+\frac{3}{L_y^2}m^2\pi^2\right)\delta(d_m-c_m)+\frac{12b}{L_x^2}\pi^2\delta d_m+8b\pi\sum_{n,g}\frac{\frac{1}{2L_y^2}(g^2+n^2-m^2)c_g d_n-2(g^2+n^2)-\frac{4}{L_x^2}c_g d_n}{(n\pm g\pm m)}gmn \tag{65}$$

where $b=L_x^2L_y^2/(2i\sigma L_x^2L_y^2+4\pi^2L_y^2+m^2\pi^2L_x^2)$

$$h_m=c\left(i\sigma+\frac{12}{L_x^2}\pi^2+\frac{3m^2}{2L_y^2}\pi^2\right)\delta d_m-2c\pi\sum_{n,g}\frac{\frac{1}{L_y^2}(g^2+n^2-m^2)-\left(\frac{16}{L_x^2}+\frac{2}{L_y^2}\right)}{(n\pm g\pm m)}gmnd_g d_n \tag{66}$$

where $c=L_x^2L_y^2/(2i\sigma L_x^2L_y^2+16\pi^2L_y^2+m^2\pi^2L_x^2)$

Appendix D. FSFS

Considering the first harmonic solution as

$$a_1(x,y)=\sum_m\sum_n c_{mn}\cos\frac{m\pi x}{L_x}\sin\frac{n\pi y}{L_y} \tag{67}$$

and the second harmonic solution,

$$a_2(x,y)=\sum_r\sum_s d_{rs}\cos\frac{r\pi x}{L_x}\sin\frac{s\pi y}{L_y} \tag{68}$$

the coefficients of the infinite series can be found as

$$d_{rs}=\sum_a d_{rs}^{(a)} \tag{69}$$

where

$$d_{rs}^{(1)}=\frac{\pi}{L_x^2}\sum_{m,n,g,h}\frac{4m^2ng^2hrsc_{mn}c_{gh}}{(s\pm n\pm h)(r\pm m\pm g)}$$

$$d_{rs}^{(2)}=3\delta\frac{\pi}{L_x^2}\sum_{m,n}\frac{m^2c_{mn}(r^2+1-m^2)}{(n+s)(r\pm m\pm 1)}$$

$$d_{rs}^{(3)}=3\delta\sum_{m,n}\frac{m^2c_{mn}(1-r^2-m^2)}{\pi(n+s)(\pm r+m\pm 1)}$$

$$d_{rs}^{(4)}=-\frac{\pi^2}{L_x^2}\sum_{m,n,g,h}\frac{2rgmnhsg^2c_{mn}c_{gh}}{(\pm s+n\pm h)(\pm r+m\pm g)}$$

$$d_{rs}^{(5)}=\frac{3\delta}{L_y^2}\sum_{m,n,g,h}\frac{-ngshc_{mn}c_{gh}(s^2-h^2-n^2)(m^2+r^2-g^2)}{(s\pm n\pm h)(r\pm m\pm g)}$$

$$d_{rs}^{(6)}=3\delta\frac{\pi}{L_y^2}\sum_{m,n}\frac{n^2c_{mn}(+m^2+r^2-1)}{(n+s)(\pm r\pm 1+m)}$$

$$d_{rs}^{(7)}=-\frac{\pi^2}{L_y^2}\sum_{m,n,g,h}\frac{-2c_{mn}h^2c_{gh}(nhs)(m)}{(s\pm n\pm h)(r\pm m+g)}$$

$$d_{rs}^{(8)}=-2j\sigma\delta\sum_{m,n}\frac{-c_{mn}(-1+m^2+r^2)}{\pi(n+s)(r\pm 1\pm m)} \tag{70}$$

and m,g,r are even numbers, n,h,s are odd numbers.

Appendix E. CFFC

Considering the first harmonic solution as

$$a_1(x,y)=\sum_m\sum_n c_{mn}\cos\frac{m\pi x}{2L_x}\cos\frac{n\pi y}{2L_y} \tag{71}$$

and the second harmonic solution,

$$a_2(x,y)=\sum_r\sum_s d_{rs}\cos\frac{r\pi x}{2L_x}\cos\frac{s\pi y}{2L_y} \tag{72}$$

the coefficients of the infinite series can be found as $d_{rs}=\sum_a d_{rs}^{(a)}$ where

$$d_{rs}^{(1)}=\sum_{m,n,g,h}\frac{mnghrsc_{mn}c_{gh}\left(\frac{m^2-g^2-r^2}{L_x^2}+\frac{n^2-h^2-s^2}{L_y^2}\right)}{(\pm s+n\pm h)(\pm r+m\pm g)}(-1)^{(s+n+h+r+m+g-6)/2}$$

$$d_{rs}^{(2)}=-3\delta\sum_{m,n}\frac{mnrsc_{mn}(-1)^{(m+n+r+s-4)/2}}{(\pm 1+n\pm s)(\pm r+m\pm 1)}\left(\frac{1+m^2-r^2}{L_x^2}+\frac{1+n^2-s^2}{L_y^2}\right)$$

$$d_{rs}^{(3)}=-\frac{3\pi\delta}{4L_x^2}\sum_{m,n}\frac{mnrc_{mn}(1+m^2-r^2)(-1)^{(m+r+n-3)/2}}{(n+s)(\pm r+m\pm 1)}$$

$$d_{rs}^{(4)}=-\frac{3\pi\delta}{4L_y^2}\sum_{m,n}\frac{mnsc_{mn}(n^2+1-s^2)(-1)^{(s+n+m-3)/2}}{(m+r)(\pm s\pm 1+n)}$$

$$d_{rs}^{(5)}=-\frac{3\delta}{4L_x^2}\sum_{m,n}\frac{4mn(m^2+n^2)c_{mn}(-1)^{(m+n+s-3)/2}}{(\pm 1\pm m+r)(\pm 1+n\pm s)}\left(\frac{s}{m+r}+\frac{r}{n+s}\right)$$

$$d_{rs}^{(6)}=-\sum_{m,n}\frac{mn\delta\left(\frac{2j\sigma}{\pi}+\frac{3\pi}{4L_x^2}(m^2+n^2)\right)c_{mn}(-1)^{(m+n-2)/2}}{(m+r)(n+s)}\left(\frac{1}{\pm 1\pm m+r}+\frac{1}{\pm 1\pm s+n}\right)$$

$$d_{rs}^{(7)}=8j\sigma\delta\sum_{m,n}\frac{mnc_{mn}(-1)^{(r+m-2)/2}}{\pi^2(\pm 1\pm s+n)(\pm 1\pm r+m)}\left(\frac{r}{s+n}+\frac{s}{m+r}\right) \tag{73}$$

and m,n,r,s are odd numbers.

Appendix F. FFFC

Considering the first harmonic solution as

$$a_1(x,y)=\sum_m\sum_n c_{mn}\cos\frac{m\pi x}{2L_x}\sin\frac{n\pi y}{L_y} \tag{74}$$

and the second harmonic solution,

$$a_2(x,y)=\sum_r\sum_s d_{rs}\cos\frac{r\pi x}{2L_x}\sin\frac{s\pi y}{L_y} \tag{75}$$

the coefficients of the infinite series can be found as $d_{rs}=\sum_a d_{rs}^{(a)}$ where

$$d_{rs}^{(1)}=\frac{1}{L_x^2}\sum_{m,n,g,h}\frac{mnghrsc_{mn}c_{gh}(m^2-r^2-g^2)}{(\pm s+n\pm h)(r\pm m\pm g)}(-1)^{(r+m+g-3)/2}$$

$$d_{rs}^{(2)}=\frac{2}{L_y^2}\sum_{m,n,g,h}\frac{nhrsc_{mn}c_{gh}(n^2+h^2-s^2)(m^2+g^2-r^2)}{(\pm s+n\pm h)(\pm r+m\pm g)}(-1)^{(r+m+g-3)/2}$$

$$d_{rs}^{(3)}=-\frac{8}{L_y^2}\sum_{m,n,g,h}\frac{mn^3ghrsc_{mn}c_{gh}}{(s\pm n\pm h)(\pm r\pm m+g)}(-1)^{(r+m+g-3)/2}$$

$$d_{rs}^{(4)}=3\delta\frac{\pi}{4L_x^2}\sum_{m,n}\frac{mrc_{mn}(m^2+1-r^2)}{(\pm r\pm 1+m)(n+s)}$$

$$d_{rs}^{(5)}=-3\delta\frac{\pi^2}{4L_x^2}\sum_{m,n}\frac{2r(m+r)+(\pm 1+m\pm r)}{\pi(m+r)(n+s)(\pm 1+m\pm r)}sm^3c_{mn}(-1)^{(m+r-2)/2}$$

$$d_{rs}^{(6)}=-3\delta\frac{\pi^2}{L_y^2}\sum_{m,n}\frac{(\pm 1+m\pm r)\frac{\pi}{2}+2m(m+r)(-1)^{(m+r-2)/2}}{\pi(m+r)(n+s)(\pm 1+m\pm r)}n^2rsc_{mn}$$

$$d_{rs}^{(7)} = -2j\sigma\delta\sum_{m,n}\frac{2r(m+r)+(\pm 1+m\pm r)\frac{\pi}{2}}{\pi(m+r)(n+s)(\pm 1+m\pm r)}smc_{mn}(-1)^{(r+m-2)/2} \tag{76}$$

and m,n,g,h,r,s are odd numbers.

References

[1] W. Jung, Y. Peter, J. Wang, O. Solgaard, Single-crystal-silicon continuous membrane deformable mirror array for adaptive optics in space-based telescopes, *IEEE Journal of Selected Topics in Quantum Electronics* 13 (2) (2007) 162–167.
[2] W.E. Langlois, Isothermal squeeze films, *Quarterly Applied Mathematics* 20 (2) (1962) 131–150.
[3] R.B. Darling, C. Hivick, J. Xu, Compact analytical modeling of squeeze film damping with arbitrary venting conditions using a Green's function approach, *Sensors and Actuators A: Physical* 70 (1–2) (1998) 32–41.
[4] U.K. Ingard, A. Akay, On the vibration damping of a plate by means of a viscous fluid layer, *ASME Journal of Vibration, Acoustics, Stress and Reliability in Design* 109 (2) (1987) 178–184.
[5] L.C. Chow, R.J. Pinnington, Practical industrial method of increasing structural damping in machinery, I: squeeze-film damping with air, *Journal of Sound and Vibration* 118 (1) (1987) 123–139.
[6] G. Maidanik, E.E. Ungar, Panel Loss Factors due to Gas-pumping at Structural Joints, NASA, 1967.
[7] T. Onsay, Dynamic interactions between the bending vibrations of a plate and a fluid layer attenuator, *Journal of Sound and Vibration* 178 (3) (1994) 289–313.
[8] M.J.H. Fox, P.N. Whitton, The damping of structural vibrations by thin gas films, *Journal of Sound and Vibration* 73 (1980) 279–295.
[9] W.M. Beltman, Viscothermal wave propagation including acousto-elastic interaction, Part I: theory, *Journal of Sound and Vibration* 227 (3) (1999) 555–586.
[10] W.M. Beltman, P.J.M. Van der Hoogt, R.M.E.J. Spiering, H. Tijdeman, Implementation and experimental validation of a new viscothermal acoustic finite element for acousto-elastic problems, *Journal of Sound and Vibration* 216 (1) (1998) 159–185.
[11] T.G.H. Basten, P.J.M. Van Der Hoogt, R.M.E.J. Spiering, H. Tijdeman, On the acousto-elastic behaviour of double-wall panels with a viscothermal air layer, *Journal of Sound and Vibration* 243 (4) (2001) 699–719.
[12] A. Akrout, L. Hammami, M.B. Tahar, M. Haddar, Vibro-acoustic behaviour of laminated double glazing enclosing a viscothermal fluid cavity, *Applied Acoustics* 70 (1) (2009) 82–96.
[13] C. Lei, R.D. White, K. Grosh, Three-dimensional viscous finite element formulation for acoustic fluid–structure interaction, *Computer Methods in Applied Mechanics and Engineering* 197 (49–50) (2008) 4160–4172.
[14] A. Akrout, C. Karra, L. Hammami, M. Haddar, Viscothermal fluid effects on vibro-acoustic behaviour of double elastic panels, *International Journal of Mechanical Sciences* 50 (4) (2008) 764–773.
[15] T. Le Van Suu, P. Honzik, S. Durand, N. Joly, Z. Skvor, M. Bruneau, Thin film thermo-viscous damping in miniature condenser microphones, *The Journal of the Acoustical Society of America* 123 (5) (2008) 3229.
[16] Y.J. Yang, M.A. Gretillat, S.D. Senturia, Effect of air damping on the dynamics of nonuniform deformations of microstructures, *1997 International Conference on Solid State Sensors and Actuators*, *TRANSDUCERS '97*, Vol. 2, Chicago, 1997, pp. 1093–1096.
[17] A.H. Nayfeh, M.I. Younis, A new approach to the modeling and simulation of flexible microstructures under the effect of squeeze-film damping, *Journal of Micromechanics and Microengineering* 14 (2) (2004) 170–181.
[18] J.B. Starr, Squeeze-film damping in solid-state accelerometers, *4th Technical Digest, IEEE Solid-State Sensor and Actuator Workshop, 1990*, 1990, pp. 44–47.
[19] M.H. Sadd, A.K. Stiffer, Squeeze film dampers: amplitude effects at low squeeze numbers, *Journal of Engineering for Industry-Transactions of the ASME, Series B* (97) (1975) 1366–1370.
[20] M. Bao, H. Yang, Squeeze film air damping in MEMS, *Sensors and Actuators: A Physical* 136 (1) (2007) 3–27.
[21] P.Y. Kwok, M.S. Weinberg, K.S. Breuer, Fluid effects in vibrating micromachined structures, *Journal of MicroElectroMechanical Systems* 14 (4) (2005) 770–781.
[22] D. Homentcovschi, R.N. Miles, Viscous damping of perforated planar micromechanical structures, *Sensors and Actuators A: Physical* 119 (2) (2005) 544–552.
[23] W.A. Gross, *Gas Film Lubrication*, John Wiley, New York, 1962.
[24] S. Beltman, W.M. Basten, T.G.H. Basten, H. Tijdeman, Viscothermal damping in thin gas or fluid layers, *Adaptive structures and material systems*, American Society of Mechanical Engineers, New York, 1999, pp. 387–395. ISBN 9780791816424.
[25] T. Veijola, H. Kuisma, J. Lahdenperä, T. Ryhänen, Equivalent-circuit model of the squeezed gas film in a silicon accelerometer, *Sensors and Actuators A: Physical* 48 (3) (1995) 239–248.
[26] Y.T. Hsia, G.A. Domoto, An experimental investigation of molecular rarefication effects in gas lubricated bearing at ultra-low clearance, *Journal of Tribology-Transactions of the ASME* 105 (1983) 120–130.
[27] W.S. Griffin, H.H. Richardson, S. Yamanami, A study of fluid squeeze-film damping, *ASME Journal of Basic Engineering* (1966) 451–456.
[28] A.W. Leissa, Vibration of Plates, NASA, 1969.